Analysis of Relative Motion in Non-Keplerian Orbits via Modified Equinoctial Elements

Wei Wang[(1)], Giovanni Mengali[(2)], Alessandro A. Quarta[(2)],*

Jianping Yuan[(1)]

[(1)] *National Key Laboratory of Aerospace of Flight Dynamics, Northwestern Polytechnical University, 710072 Xi'an, People's Republic of China*

[(2)] *Department of Civil and Industrial Engineering, University of Pisa, I-56122 Pisa, Italy*

Abstract

This paper discusses a mathematical model to determine an analytical form of the equations describing the relative motion of two spacecraft that, using a suitable continuous-thrust propulsion system, track highly non-Keplerian orbits, whose orbital plane does not contain the primary's center-of-mass. The relative motion is described within a rotating reference frame via modified equinoctial elements, thus eliminating the singularities that arise when a set of classical orbital elements is used. In this sense, the paper completes and extends the recent analysis of the relative motion of two spacecraft in closed (either circular or elliptic) displaced orbits. When the eccentricity of the displaced orbits are sufficiently small, the method is able to calculate the approximate bounds of the two spacecraft relative distances using a semi-analytical approach and with a reduced computational effort. Some numerical simulation results provide an evidence of the effectiveness of the proposed method.

Key words: non-Keplerian orbits, formation flying, nonsingular elements

Nomenclature

a	=	semimajor axis of displaced orbit, [au]
E	=	eccentric anomaly, [rad]
e	=	eccentricity
f, g, h, k	=	modified equinoctial elements
H	=	orbital displacement, [au]
i	=	inclination of displaced orbit, [rad]
K	=	eccentric longitude, [rad]
L	=	true longitude, [rad]
l	=	mean longitude, [rad]
M	=	mean anomaly, [rad]
n	=	mean motion, [rad/day]
O	=	Sun's center-of-mass
o	=	focus of displaced orbit
p	=	semilatus rectum of displaced orbit, [au]
$\boldsymbol{r}$	=	spacecraft inertial position vector (with $r \triangleq \|\boldsymbol{r}\|$), [au]
S	=	spacecraft center-of-mass
s	=	auxiliary variable, see Eq. (54)
t	=	time, [days]

* Corresponding author.

Email addresses: 418362467@qq.com (Wei Wang[(1)]), g.mengali@ing.unipi.it (Giovanni Mengali[(2)]), a.quarta@ing.unipi.it (Alessandro A. Quarta[(2)],), jyuan@nwpu.edu.cn (Jianping Yuan[(1)]).

$\mathcal{T}$	=	reference frame
$\mathbb{T}_{EI}$	=	transformation matrix between $\mathcal{T}_E$ and $\mathcal{T}_I$
$\mathbb{T}_{ER}$	=	transformation matrix between $\mathcal{T}_E$ and $\mathcal{T}_R$
$\mathbb{T}$	=	transformation matrix between $\mathcal{T}_{E_D}$ and $\mathcal{T}_{E_C}$
T_{ij}	=	(i, j) entry of matrix $\mathbb{T}$
$\hat{\boldsymbol{x}},\ \hat{\boldsymbol{y}},\ \hat{\boldsymbol{z}}$	=	unit vector of x, y and z-axis
$\zeta, \eta, \kappa, \lambda, \sigma, \tau$	=	auxiliary (constant) coefficients
$\iota,\ \upsilon$	=	auxiliary variables, see Eqs. (34)
$\mu_\odot$	=	Sun's gravitational parameter, $[\,\mathrm{au}^3/\mathrm{day}^2]$
ν	=	true anomaly, [rad]
$\boldsymbol{\rho}$	=	relative position vector, [au]
$\rho_x,\ \rho_y,\ \rho_z$	=	components of relative position vector in the chief's rotating frame, [au]
Ω	=	right ascension of the ascending node of displaced orbit, [rad]
ω	=	argument of periapsis of displaced orbit, [rad]

Subscripts

C	=	chief
D	=	deputy
E	=	equinoctial
I	=	inertial
R	=	rotating

Superscripts

$\star$	=	extreme value
$\wedge$	=	unit vector

1 Introduction

A growing interest towards highly non-Keplerian orbits, that is, closed orbits whose shape is considerably affected by the propulsive acceleration of the primary propulsion system, has arisen in recent years due to their peculiarities in astronomical observations both in a heliocentric and in a planetocentric mission scenario [1]. In this context, displaced orbits, that is, orbits whose orbital plane does not contain the primary's center-of-mass, have been proposed in mission applications that involve monitoring either solar plasma storms [2] or planetary polar regions [3]. In particular, the use of displaced orbits has been analyzed as a feasible option for the deflection of potentially dangerous asteroids by means of the gravity tractor concept [4,5]. The basic idea is that a spacecraft with a non-negligible mass is maintained at a prescribed distance from the asteroid by a continuous thrust propulsion system using a suitable control law [6], in order to change the heliocentric orbital parameters of the asteroid by exploiting the gravitational coupling. Another interesting mission scenario involving displaced orbits is offered by a novel concept for an Earth-Mars interplanetary communications relay [7] in support of a future manned mission toward Mars. In that case, a spacecraft that covers a displaced orbit with respect to the ecliptic plane, could be used for communicating with Earth when Mars is occulted by the Sun. A similar idea could, in principle, be used to build a support network for communication purposes in a hypothetical manned mission toward one of the near-Earth asteroids whose orbit lies approximately on the ecliptic plane [8].

Those mission scenarios require a continuous propulsive acceleration to maintain a desired orbit's displacement for a time-span on the order of some terrestrial years. With the development of advanced propulsion systems, such as photonic solar sails [9,10] or the more recent electric solar wind sails [11,12], the planning of displaced orbits can be considered a feasible option during the preliminary analysis of a scientific space mission. However, the small thrust capabilities of these propulsion systems, combined with the medium-high values of propulsive acceleration required to maintain those displaced orbits, implies the need of using payloads with a modest mass only. A possible solution to this problem consists in distributing the payload among multiple spacecraft operating in a formation flight. The formation flight concept can also be used to create a large virtual sensor, capable of providing a resolution enhancement for the purpose of multi-aspect observations. A suitable analysis of the spacecraft formation flying dynamics and the study of the relative motion of two (or more) spacecraft that nominally track displaced orbits of given characteristics represents an important and challenging problem. In this context, the knowledge of the bounds (i.e., the maximum and minimum values) of the relative motion is of great importance, since the upper bounds are essential for communication purposes, while the lower bounds are crucial for collision avoidance.

Previous work on this subject has been devoted to investigate the relative motion of solar sails around displaced orbits [13,14], under the assumption that the chief spacecraft covers a circular reference orbit, while the deputy adjusts its thrust angle so as to follow a trajectory of given characteristics. However, the necessary active control strategy requires a full relative state measurement, which unavoidably complicates the control system design, especially for

solar sails with a large and complex (gossamer) structure. A substantial simplification is to assume a passive control, i.e. a control system that exploits the natural tendency of a solar sail, of suitable shape, to maintain its attitude with respect to a classical orbital reference frame. In this case the problem of relative motion between two spacecraft that cover circular displaced orbits has been firstly analyzed in Ref. [15] using a purely geometrical approach. It has been found that the relative motion evolves on its invariant manifold, which can be parameterized by means of a set of new displaced orbital elements that closely resemble the classical orbital elements. Recently, the study has been extended to include the case of elliptic displaced orbits [16], where, under the assumption of a small orbital eccentricity, semi-analytical approximations have been found for calculating the extreme distances of two spacecraft as a function of the shape and orientation of the two displaced orbits involved in the problem.

Similar to what happens with the classic orbital elements, the displaced elements introduced in Refs. [15,16] to describe the displaced orbits show inherent singularities, since the right ascension of the ascending node (or the argument of perigee) becomes undefined as the orbital inclination (or the orbital eccentricity) tends to zero. Such a problem calls for a regularization procedure and, in this context, many different choices are available to solve the problem [17], including the Kustaanheimo-Stiefel (KS) elements, quaternion elements, canonical elements, and Euler parameters [18]. Among them, an interesting (and widely adopted) option is provided by the modified equinoctial elements [19,20] which, due to their clear physical interpretation, are commonly used to eliminate the singularities and to derive the planetary equations for arbitrarily high-order gravitational harmonics. This is exactly the

choice adopted in this work to describe the motion of two spacecraft along highly non-Keplerian (displaced) orbits and to circumvent the singularities of the model discussed in Refs. [15,16]. Accordingly, this paper provides a comprehensive analysis of closed-form solutions and distance bounds of relative motion between two displaced orbits via modified equinoctial elements, thus unifying the recently developed formalisms, wherein the relative motion in circular case [15] and elliptic case [16] have been studied separately.

The relative motion is formulated in a suitable rotating reference frame that tracks the flight of one of the two spacecraft. In this framework, an analytical (exact) expression of the relative distance is obtained, in terms of modified equinoctial elements, using a sequence of coordinate transformations and a geometrical approach. Paralleling the procedure introduced in Refs. [15,16], this paper show that, using a suitable reference frame and a clever choice of angular coordinates, the approximate extreme values of the relative distances in the radial, along-track and cross-track directions can be analytically calculated as a function of the modified equinoctial elements. In the latter case, however, the semi-analytical approach requires the evaluation of the roots of some algebraic equations that, in general, need a set of guess values. Nevertheless, the use of standard root finding methods allows the numerical procedure to be quick and efficient compared to a classical numerical integration of the equations of motion.

Even though the methodology illustrated in this paper follows the approach discussed in Refs. [15,16], it is worth noting that the use of nonsingular parameters requires a significant change of the mathematical model as well as a complexity increase, especially for what concerns the approximate algebraic relations that allows the extreme values of the relative distance to be found.

Accordingly, the main contribution of this paper is in the generalization of the mathematical procedure that avoids any failure even when the previous models were defective. The usefulness of the model discussed in this paper is emphasized by means of suitable mission scenarios involving orbits that would be difficult to analyze with the previous discussed models [15,16].

2 Problem Formulation

Consider a spacecraft that tracks a (closed) displaced orbit around the Sun , with a given eccentricity $e < 1$ and a given semimajor axis a or, equivalently, a given semilatus rectum p, see Fig. 1. The figure also shows an International Celestial Reference Frame J2000.0 (ICRF/J2000.0) $\mathcal{T}_I\,(O; \hat{\boldsymbol{x}}_I, \hat{\boldsymbol{y}}_I, \hat{\boldsymbol{z}}_I)$ and a rotating reference frame $\mathcal{T}_R\,(S; \hat{\boldsymbol{x}}_R, \hat{\boldsymbol{y}}_R, \hat{\boldsymbol{z}}_R)$. In particular, the origin O of $\mathcal{T}_I$ is at the Sun's center-of-mass, the unit vector $\hat{\boldsymbol{x}}_I$ is directed from O to the vernal equinox, and $\hat{\boldsymbol{z}}_I$ points to the celestial north pole. The frame $\mathcal{T}_R$ is centered at the spacecraft center-of-mass S, which belongs to a plane $\mathcal{P}$ placed at a distance H from the Sun's center-of-mass O, the unit vector $\hat{\boldsymbol{x}}_R$ is in the radially outward direction from the focus of the displaced orbit o to S, $\hat{\boldsymbol{z}}_R$ is normal to the plane $\mathcal{P}$ and is positive in the direction of the spacecraft angular velocity vector. Note that the plane $\mathcal{P}$ and the focus o are both assumed to be fixed in time.

In previous studies [15,16], the spacecraft position has been expressed by means of a set of displaced orbital elements $\{a,\, e,\, i,\, \Omega,\, \omega,\, \nu,\, H\}$, where the true anomaly ν is measured anticlockwise from the line connecting the orbital focus o with the pericenter of the displaced orbit, the inclination i is the angle between the direction of $\hat{\boldsymbol{z}}_I$ and the O-o line, the argument of periapsis ω is

defined as the angle between the line of nodes (i.e., the intersection of $\mathcal{P}$ with the plane $\mathcal{E}$ containing the orbital focus o and parallel to the ecliptic plane) and the direction of the periapsis, and the right ascension of the ascending node Ω is the angle measured from the direction of $\hat{\boldsymbol{x}}_I$ to the line of nodes.

As is well known, the angle Ω is undefined when the inclination i becomes zero, whereas ω is indeterminate when the eccentricity e is zero. This intrinsic limitation of the (classical) orbital elements-based approach, restricts the applicability of the mathematical model discussed in Ref. [16]. In particular, the singularity of Ω prevents the application of the semi-analytical model proposed in Ref. [16] when the spacecraft has to maintain a constant displacement above (or below) the ecliptic plane. This is an important case, as is representative of a mission scenario in which the spacecraft tracks a celestial body whose orbit is close to the ecliptic plane as happens, for example, for some near-Earth objects [21,22] or the Earth itself. According to Refs. [19,20], these singularities can be eliminated by introducing the set of modified equinoctial elements $\{p,\, f,\, g,\, h,\, k,\, L\}$ defined as

$$p = a\,\left(1 - e^2\right) \tag{1}$$

$$f = e\,\cos\left(\Omega + \omega\right) \tag{2}$$

$$g = e\,\sin\left(\Omega + \omega\right) \tag{3}$$

$$h = \cos\Omega\,\tan(i/2) \tag{4}$$

$$k = \sin\Omega\,\tan(i/2) \tag{5}$$

$$L = \Omega + \omega + \nu \tag{6}$$

and using [23] an equinoctial reference frame $\mathcal{T}_E\left(S; \hat{\boldsymbol{x}}_E, \hat{\boldsymbol{y}}_E, \hat{\boldsymbol{z}}_E\right)$, whose axes

are obtained by performing a negative rotation of the rotating frame $\mathcal{T}_R$, about z_R-axis, of an angle equal to the true longitude L, see Fig. 1. Let $\boldsymbol{r}$ be the absolute spacecraft position vector, i.e., the vector from the Sun's center-of-mass O to the spacecraft's center-of-mass S. Its components in the rotating frame $\mathcal{T}_R$ can be written as a function of the true longitude L as

$$[\boldsymbol{r}]_{\mathcal{T}_R} = \left[\frac{p}{1 + f\,\cos L + g\,\sin L}, \quad 0, \quad H\right]^{\mathrm{T}} \tag{7}$$

whereas the components of $\boldsymbol{r}$ in the equinoctial frame $\mathcal{T}_E$ are [23]

$$[\boldsymbol{r}]_{\mathcal{T}_E} = \begin{bmatrix} \dfrac{p}{1-f^2-g^2}\left[\left(1 - \dfrac{g^2}{1+\sqrt{1-f^2-g^2}}\right)\cos K + \dfrac{f\,g}{1+\sqrt{1-f^2-g^2}}\sin K - f\right] \\ \dfrac{p}{1-f^2-g^2}\left[\left(1 - \dfrac{f^2}{1+\sqrt{1-f^2-g^2}}\right)\sin K + \dfrac{f\,g}{1+\sqrt{1-f^2-g^2}}\cos K - g\right] \\ H \end{bmatrix} \tag{8}$$

where K is the so called eccentric longitude [23], defined as

$$K \triangleq \Omega + \omega + E \tag{9}$$

while E is the eccentric anomaly of the displaced (closed) orbit. Note that the eccentric longitude K can be used in place of the true longitude L by exploiting the equations

$$\cos L = \frac{1}{1 - f\,\cos K - g\,\sin K}\left[\left(1 - \frac{g^2}{1+\sqrt{1-f^2-g^2}}\right)\cos K + \frac{f\,g}{1+\sqrt{1-f^2-g^2}}\sin K - f\right] \tag{10}$$

$$\sin L = \frac{1}{1 - f\,\cos K - g\,\sin K}\left[\left(1 - \frac{f^2}{1+\sqrt{1-f^2-g^2}}\right)\sin K + \frac{f\,g}{1+\sqrt{1-f^2-g^2}}\cos K - g\right] \tag{11}$$

Consider now the general case of two spacecraft tracking different closed dis-

placed orbits around the primary body (the Sun, for instance). The first spacecraft is referred to as the chief (subscript C), the other as the deputy (subscript D), see Fig. 2 . Bearing in mind Eq. (7), the components of the relative position vector

$$\boldsymbol{\rho} \triangleq \boldsymbol{r}_D - \boldsymbol{r}_C \tag{12}$$

in the chief's rotating reference frame $\mathcal{T}_{R_C}$ can be calculated once the components of vector $\boldsymbol{r}_D$ are known in $\mathcal{T}_{R_C}$. To this end, extending the procedure described in Ref. [16], three concatenated coordinate transformations are performed, viz. $\mathcal{T}_{E_D} \rightarrow \mathcal{T}_I \rightarrow \mathcal{T}_{E_C} \rightarrow \mathcal{T}_{R_C}$.

Let $\mathbb{T}_{EI}$ be the transformation matrix from frame $\mathcal{T}_R$ to frame $\mathcal{T}_I$, which can be written as a function of $\{h,\, k\}$ as [23]

$$\mathbb{T}_{EI}\,(h,k) = \frac{1}{1+h^2\,+k^2} \begin{bmatrix} 1+h^2-k^2 & 2\,h\,k & 2\,k \\ 2\,h\,k & 1-h^2+k^2 & -2\,h \\ -2\,k & 2\,h & 1-h^2-k^2 \end{bmatrix} \tag{13}$$

and $\mathbb{T}_{ER}$ is the transformation matrix from frame $\mathcal{T}_E$ to frame $\mathcal{T}_R$

$$\mathbb{T}_{ER}\,(L) = \begin{bmatrix} \cos L & \sin L & 0 \\ -\sin L & \cos L & 0 \\ 0 & 0 & 1 \end{bmatrix} \tag{14}$$

Accordingly, the relative position vector $\boldsymbol{\rho}$ in the chief's rotating reference frame $\mathcal{T}_{R_C}$ is

$$[\boldsymbol{\rho}]_{\mathcal{T}_{R_C}} = \mathbb{T}_{ER}(L_C)\,\mathbb{T}_{EI}^{\mathrm{T}}\,(h_C,k_C)\;\mathbb{T}_{EI}\,(h_D,k_D)\;[\boldsymbol{r}_D]_{\mathcal{T}_{E_D}} - [\boldsymbol{r}_C]_{\mathcal{T}_{R_C}} \tag{15}$$

where $[\boldsymbol{r}_D]_{\mathcal{T}_{E_D}}$ is a function of the set $\{p_D, f_D, g_D, H_D, L_D\}$ via Eqs. (8), (10) and (11), whereas $[\boldsymbol{r}_C]_{\mathcal{T}_{R_C}}$ is a function of the set $\{p_C, f_C, g_C, H_C, L_C\}$ via Eq. (7). For brevity, the eccentric longitude K_D is now used in place of the true longitude L_D for the deputy, and the following shorthand notation is introduced

$$\mathbb{T} \triangleq \mathbb{T}_{EI}^{\mathrm{T}}\left(h_C, k_C\right)\, \mathbb{T}_{EI}\left(h_D, k_D\right) \tag{16}$$

where $\mathbb{T}$ represents the transformation matrix (with generic entry T_{ij}) from frame $\mathcal{T}_{E_D}$ to frame $\mathcal{T}_{E_C}$.

Substituting Eqs. (7), (10) and (13)-(14) into Eq. (15), after some algebraic manipulations the three components ρ_x, ρ_y and ρ_z of vector $\boldsymbol{\rho}$ are expressed in the chief's rotating reference frame as

$$\begin{aligned}\rho_x = {} & \lambda_1 \cos L_C \cos K_D + \lambda_2 \sin L_C \cos K_D + \lambda_3 \cos L_C \sin K_D + \lambda_4 \sin L_C \sin K_D \\ & + \lambda_5 \cos L_C + \lambda_6 \sin L_C - \frac{p_C}{1 + f_C \cos L_C + g_C \sin L_C}\end{aligned} \tag{17}$$

$$\begin{aligned}\rho_y = {} & \lambda_2 \cos L_C \cos K_D - \lambda_1 \sin L_C \cos K_D + \lambda_4 \cos L_C \sin K_D - \lambda_3 \sin L_C \sin K_D \\ & + \lambda_6 \cos L_C - \lambda_5 \sin L_C\end{aligned} \tag{18}$$

$$\rho_z = \lambda_7 \cos K_D + \lambda_8 \sin K_D + \lambda_9 \tag{19}$$

where the coefficients λ_1, λ_2, $\ldots$, λ_9 depend on the modified orbital elements

that define the shape and orientations of the two displaced orbits, viz.

$$\lambda_1 \triangleq \frac{p_D}{1-f_D^2-g_D^2}\left[\left(1-\frac{g_D^2}{1+\sqrt{1-f_D^2-g_D^2}}\right)T_{11}+\frac{f_D\,g_D}{1+\sqrt{1-f_D^2-g_D^2}}\,T_{12}\right] \tag{20}$$

$$\lambda_2 \triangleq \frac{p_D}{1-f_D^2-g_D^2}\left[\left(1-\frac{g_D^2}{1+\sqrt{1-f_D^2-g_D^2}}\right)T_{21}+\frac{f_D\,g_D}{1+\sqrt{1-f_D^2-g_D^2}}\,T_{22}\right] \tag{21}$$

$$\lambda_3 \triangleq \frac{p_D}{1-f_D^2-g_D^2}\left[\left(1-\frac{f_D^2}{1+\sqrt{1-f_D^2-g_D^2}}\right)T_{12}+\frac{f_D\,g_D}{1+\sqrt{1-f_D^2-g_D^2}}\,T_{11}\right] \tag{22}$$

$$\lambda_4 \triangleq \frac{p_D}{1-f_D^2-g_D^2}\left[\left(1-\frac{f_D^2}{1+\sqrt{1-f_D^2-g_D^2}}\right)T_{22}+\frac{f_D\,g_D}{1+\sqrt{1-f_D^2-g_D^2}}\,T_{21}\right] \tag{23}$$

$$\lambda_5 \triangleq H_D\,T_{13}-\frac{p_D\,(T_{11}\,f_D+T_{12}\,g_D)}{1-f_D^2-g_D^2} \tag{24}$$

$$\lambda_6 \triangleq H_D\,T_{23}-\frac{p_D\,(T_{21}\,f_D+T_{22}\,g_D)}{1-f_D^2-g_D^2} \tag{25}$$

$$\lambda_7 \triangleq \frac{p_D}{1-f_D^2-g_D^2}\left[\left(1-\frac{g_D^2}{1+\sqrt{1-f_D^2-g_D^2}}\right)T_{31}+\frac{f_D\,g_D}{1+\sqrt{1-f_D^2-g_D^2}}\,T_{32}\right] \tag{26}$$

$$\lambda_8 \triangleq \frac{p_D}{1-f_D^2-g_D^2}\left[\left(1-\frac{f_D^2}{1+\sqrt{1-f_D^2-g_D^2}}\right)T_{32}+\frac{f_D\,g_D}{1+\sqrt{1-f_D^2-g_D^2}}\,T_{31}\right] \tag{27}$$

$$\lambda_9 \triangleq H_D\,T_{33}-H_C-\frac{p_D\,T_{32}\,g_D}{1-f_D^2-g_D^2} \tag{28}$$

Equations (17)–(19) provide the general (closed form) solution to the relative

motion between two spacecraft flying along two different displaced closed orbits in terms of modified equinoctial elements. Note that, unlike the displaced orbit's orbital elements discussed in Refs. [15,16], Eqs. (17)–(19) hold both in the circular case and/or in the zero-inclination case. Moreover, Eqs. (17)–(19) can also be conveniently used to analyze the relative motion of a spacecraft with respect to a celestial body (the latter can be either a planet or an asteroid). In fact, assuming that the celestial body plays the role of the chief body within the mathematical model, its motion turns out to be Keplerian by simply enforcing the condition $H_C = 0$ in Eq. (28). In that particular case, the deputy spacecraft tracks a displaced orbit as long as $H_D \neq 0$.

3 Bounds of Relative Motion

The analysis of relative motion through a geometrical approach provides an useful analytical tool for evaluating the bounds of relative distances, that is, the extreme values of each component ρ_x, ρ_y and ρ_z of the relative position vector. These extreme values can be calculated by investigating two qualitatively different cases, depending on whether the relative motion of the two spacecraft are periodic or quasi-periodic [16]. In particular, the periodic case happens when the ratio of the mean motions of the two spacecraft (n_C for the chief and n_D for the deputy) is a rational number. On the other hand, in the quasi-periodic case, the ratio n_C/n_D is an irrational number. In both cases, the relative motion evolves on its invariant manifold described by the angular coordinates (L_C, K_D). The parametric equations of the three components, ρ_x, ρ_y and ρ_z, in terms of equinoctial elements, also serve as the basis for calculating the extreme values of the relative distances for both cases, as

is illustrated in the following sections. The following results can be thought of as an extension and a completion of the results discussed in Ref. [16], where the classical orbital parameters have been used.

3.1 Quasi-periodic motion

As far as the quasi-periodic case is concerned, i.e. when the ratio n_C/n_D is an irrational number, the relative motion evolving on the invariant manifold is open, though it takes place within a well-defined region characterized by an upper and a lower bound (recall that the two displaced orbits are closed by assumption). Such a relative motion has an ergodic feature related to its topology, meaning that each orbit winds endlessly, but never intersects itself. The trajectory in this case is termed dense, because each orbit evolves arbitrarily close to (rather than passing through) each point on its invariant manifold.

When the extreme values of the relative distances are sought, the time cannot be chosen as the independent variable, since the relative motion approaches its bounds as the time tends to infinity. For this reason, the angular variables L_C and K_D in Eqs. (17)–(19) are treated as independent of each other when differentiating the relative distances with respect to them. Therefore, according to the procedure described in Refs. [15,16], the following necessary conditions should be met to find the extreme values along each coordinate axis:

$$\frac{\partial \rho_i}{\partial L_C} = 0 \qquad \text{and} \qquad \frac{\partial \rho_i}{\partial K_D} = 0 \qquad \text{with} \qquad i = \{x,\, y,\, z\} \tag{29}$$

The critical values of the chief's true longitude and deputy's eccentric longitude that solve Eq. (29) are denoted as $L_C = L_C^\star$ and $K_D = K_D^\star$, respectively, whereas the corresponding extreme values of the relative distances can be

found from Eqs. (17)–(19).

Regarding the radial distance bounds given by the extreme values of ρ_x, see Eq. (17), the necessary conditions are

$$\frac{\partial \rho_x}{\partial L_C} = 0 \qquad \text{and} \qquad \frac{\partial \rho_x}{\partial K_D} = 0 \tag{30}$$

In this case, a closed-form solution to $L_C^\star$ cannot be recovered. However, assuming that $f_C \ll 1$ and $g_C \ll 1$, that is, assuming that the eccentricity e_C of the chief's displaced orbit is sufficiently small, the last term in Eq. (17) can be approximated by a first order truncation of the Taylor series expansion, viz.

$$\frac{p_C}{1 + f_C \cos L_C + g_C \sin L_C} \simeq p_C \left(1 - f_C \cos L_C - g_C \sin L_C\right) \tag{31}$$

Based on the preliminary simulation analyses of Ref. [16], the previous approximation provides sufficiently accurate results as long as $e_C < 0.1$. Substituting Eq. (31) into Eq. (17) and enforcing the conditions of Eqs. (30), after some algebraic manipulations the result is

$$\begin{aligned} &- \lambda_1 \sin L_C \cos K_D + \lambda_2 \cos L_C \cos K_D - \lambda_3 \sin L_C \sin K_D \\ &+ \lambda_4 \cos L_C \sin K_D - (\lambda_5 + p_C f_C) \sin L_C + (\lambda_6 + p_C g_C) \cos L_C = 0 \end{aligned} \tag{32}$$

$$\lambda_4 \sin L_C \cos K_D + \lambda_3 \cos L_C \cos K_D - \lambda_2 \sin L_C \sin K_D - \lambda_1 \cos L_C \sin K_D = 0 \tag{33}$$

Using the substitution

$$\iota \triangleq \tan \frac{L_C}{2} \qquad \text{and} \qquad \upsilon \triangleq \tan \frac{K_D}{2} \tag{34}$$

Eqs. (32)-(33) can be transformed into a set of two algebraic equations, with

ι and υ being the new variables, viz.

$$(\lambda_2 - \lambda_6)\, \iota^2\, \upsilon^2 + 2\, (\lambda_1 - \lambda_5 - p_C\, f_C)\, \iota\, \upsilon^2 - 2\, \lambda_4\, \iota^2\, \upsilon - (\lambda_2 + \lambda_6)\, \iota^2 - (\lambda_2 - \lambda_6)\, \upsilon^2$$
$$- 4\, \lambda_3\, \iota\, \upsilon - 2\, (\lambda_1 + \lambda_5 + p_C\, f_C)\, \iota + 2\, \lambda_4\, \upsilon + (\lambda_2 + \lambda_6) = 0 \tag{35}$$

$$- \lambda_3\, \iota^2\, \upsilon^2 + 2\, \lambda_4\, \iota\, \upsilon^2 - 2\, \lambda_1\, \iota^2\, \upsilon + \lambda_3\, \iota^2 + \lambda_3\, \upsilon^2 + 4\, \lambda_2\, \iota\, \upsilon - 2\, \lambda_4\, \iota + 2\, \lambda_1\, \upsilon - \lambda_3 = 0 \tag{36}$$

The latter can be numerically solved as a function of ι and υ, and the critical values $L_C^\star$ and $K_D^\star$ are eventually obtained from Eq. (34).

Note, however, that the mapping $\{L_C, K_D\} \mapsto \{\iota, \upsilon\}$ is not continuous at points $L_C = k\,\pi$ and/or $K_D = k\,\pi$ (where $k \in \mathbb{N}$), because $\iota \to \pm\infty$ as $L_C \to k\,\pi$ and $\upsilon \to \pm\infty$ as $K_D \to k\,\pi$. Therefore, it is necessary to further check whether $\cos L_C = \pm 1$ and/or $\cos K_D = \pm 1$ correspond to extreme values of ρ_x by substituting them into Eq. (17).

Consider now the along-track distance bounds. Bearing in mind Eq. (18), the necessary conditions to be met are

$$\lambda_2\, \sin L_C\, \cos K_D + \lambda_1\, \cos L_C\, \cos K_D + \lambda_4\, \sin L_C\, \sin K_D + \lambda_3\, \cos L_C\, \sin K_D$$
$$+ \lambda_6\, \sin L_C + \lambda_5\, \cos L_C = 0 \tag{37}$$

$$- \lambda_3\, \sin L_C\, \cos K_D + \lambda_4\, \cos L_C\, \cos K_D + \lambda_1\, \sin L_C\, \sin K_D - \lambda_2\, \cos L_C\, \sin K_D = 0 \tag{38}$$

Using again the substitution (34), Eqs. (37) and (38) become

$$(\lambda_1 - \lambda_5)\,\iota^2\,\upsilon^2 + 2\,(\lambda_6 - \lambda_2)\,\iota\,\upsilon^2 - 2\,\lambda_3\,\iota^2\,\upsilon - (\lambda_1 + \lambda_5)\,\iota^2 - (\lambda_1 - \lambda_5)\,\upsilon^2 + 4\,\lambda_4\,\iota\,\upsilon$$
$$+ 2\,(\lambda_2 + \lambda_6)\,\iota + 2\,\lambda_3\,\upsilon + (\lambda_1 + \lambda_5) = 0 \tag{39}$$

$$\lambda_4\,\iota^2\,\upsilon^2 + 2\,\lambda_3\,\iota\,\upsilon^2 + 2\,\lambda_2\,\iota^2\,\upsilon - \lambda_4\,\iota^2 - \lambda_4\,\upsilon^2 + 4\,\lambda_1\,\iota\,\upsilon - 2\,\lambda_3\,\iota - 2\,\lambda_2\,\upsilon + \lambda_4 = 0 \tag{40}$$

Likewise, the same approach used for calculating the radial distance bounds must be adopted to check whether $\iota \to \pm\infty$ and/or $\upsilon \to \pm\infty$ actually correspond to the extreme values enforcing $\cos L_C = \pm 1$ and/or $\cos K_D = \pm 1$ into Eq. (18).

Finally, the extreme values of cross-track motion can be found by substituting Eq. (29) into Eq. (19), thus obtaining

$$-\lambda_7\,\sin K_D + \lambda_8\,\cos K_D = 0 \tag{41}$$

In this case, the critical values of the deputy's eccentric longitude corresponding to the cross-track bounds can be written in an explicit form as

$$K_D^\star = \begin{cases} (k + 1/2)\,\pi & \text{if} \quad \lambda_7 = 0 \\ \\ k\,\pi + \arctan\left(\lambda_8/\lambda_7\right) & \text{if} \quad \lambda_7 \neq 0 \end{cases} \tag{42}$$

where $k \in \mathbb{N}$. The extreme values of the cross-track relative trajectory are eventually obtained by substituting Eq. (42) into Eq. (19).

3.2 Periodic Motion

In this case, the period of the relative motion corresponds to the least common multiple of the two orbital periods. In most cases, this time-interval turns out

to be unacceptably long, with the exception of the 1:1 condition (i.e. the case in which $n_C = n_D = n$) that will now be investigated. Recalling from Eqs. (17)–(19) that the relative distances are time-implicit, it is useful to relate the true longitude and the eccentric longitude with the time to obtain a time-explicit solution. To this end, according to Battin [23], first introduce the mean longitude

$$l \triangleq \Omega + \omega + M \tag{43}$$

where M is the mean anomaly. Since $\dot{l} = \dot{M} = n$, the mean longitude can be written as

$$l = l_0 + n\ (t - t_0) \tag{44}$$

where l_0 is the mean longitude at the initial (reference) time t_0.

Bearing in mind Eqs. (6), (9) and (43)-(44), it is now sufficient to perform nonlinear mappings $L_C \mapsto t$ and $K_D \mapsto t$ using Fourier series expansions and to retain only the first terms [23]

$$\cos L \simeq -f + \cos\left(l_0 + n\,t\right) + \sqrt{f^2 + g^2}\,\cos\left(l_0 + M_0 + 2\,n\,t\right) \tag{45}$$

$$\sin L \simeq -g + \sin\left(l_0 + n\,t\right) + \sqrt{f^2 + g^2}\,\sin\left(l_0 + M_0 + 2\,n\,t\right) \tag{46}$$

$$\cos K \simeq -\frac{f}{2} + \cos\left(l_0 + n\,t\right) + \frac{\sqrt{f^2 + g^2}}{2}\cos\left(l_0 + M_0 + 2\,n\,t\right) \tag{47}$$

$$\sin K \simeq -\frac{g}{2} + \sin\left(l_0 + n\,t\right) + \frac{\sqrt{f^2 + g^2}}{2}\sin\left(l_0 + M_0 + 2\,n\,t\right) \tag{48}$$

Substituting Eqs. (45)–(48) into Eqs. (17)–(19), after some algebraic manipulations the approximate form of the relative distances can be written, as a

function of time, as

$$\rho_x \approx \sigma_0 + \sigma_1 \cos(n\,t) + \sigma_2 \sin(n\,t) + \sigma_3 \cos(2\,n\,t) + \sigma_4 \sin(2\,n\,t) + \sigma_5 \cos(3\,n\,t) + \sigma_6 \sin(3\,n\,t) \tag{49}$$

$$\rho_y \approx \tau_0 + \tau_1 \cos(n\,t) + \tau_2 \sin(n\,t) + \tau_3 \cos(2\,n\,t) + \tau_4 \sin(2\,n\,t) + \tau_5 \cos(3\,n\,t) + \tau_6 \sin(3\,n\,t) \tag{50}$$

$$\rho_z \approx \xi_0 + \xi_1 \cos(n\,t) + \xi_2 \sin(n\,t) + \xi_3 \cos(2\,n\,t) + \xi_4 \sin(2\,n\,t) \tag{51}$$

where the relevant coefficients are given in the Appendix. Equations (49)–(51) provide a first-order approximate closed-form solution that is meaningful for describing the relative motion of two spacecraft tracking two different displaced orbits and, therefore, can be used to look for the extreme values of the relative distances by enforcing the necessary condition

$$\frac{\partial \rho_i}{\partial t} = 0 \qquad \text{with} \qquad i = \{x,\, y,\, z\} \tag{52}$$

As far as the radial distance bounds are concerned, the necessary condition of Eq. (52) can be transformed from a trigonometric form into a parametric algebraic form by replacing s with t as

$$\zeta_6\, s^6 + \zeta_5\, s^5 + \zeta_4\, s^4 + \zeta_3\, s^3 + \zeta_2\, s^2 + \zeta_1\, s + \zeta_0 = 0 \tag{53}$$

where

$$s \triangleq \tan \frac{n\,t}{2} \tag{54}$$

and ζ_0, ζ_1, ..., ζ_6 are constant coefficients, given by

$$\zeta_0 = -\sigma_2 + 2\,\sigma_4 - 3\,\sigma_6 \tag{55}$$

$$\zeta_1 = 2\,\sigma_1 + 8\,\sigma_3 + 18\,\sigma_5 \tag{56}$$

$$\zeta_2 = -\sigma_2 - 10\,\sigma_4 + 45\,\sigma_6 \tag{57}$$

$$\zeta_3 = 4\,\sigma_1 - 60\,\sigma_5 \tag{58}$$

$$\zeta_4 = \sigma_2 - 10\,\sigma_4 - 45\,\sigma_6 \tag{59}$$

$$\zeta_5 = 2\,\sigma_1 - 8\,\sigma_3 + 18\,\sigma_5 \tag{60}$$

$$\zeta_6 = \sigma_2 + 2\,\sigma_4 + 3\,\sigma_6 \tag{61}$$

where σ_0, σ_1, ..., σ_6 are listed in the Appendix. Note that Eq. (53) is a sixth order polynomial equation whose real roots can be easily found using a numerical method. Accordingly, the critical times at which the radial motion reaches its boundaries are calculated from Eq. (54). Since the change of variable in Eq. (54) can only be operated provided $n\,t \neq (2\,k+1)\,\pi$ (with $k \in \mathbb{N}$), it is necessary to substitute $n\,t = (2\,k+1)\,\pi$ into Eq. (49) to further check whether $n\,t = (2\,k+1)\,\pi$ correspond to extreme values, that is, to check whether Eq. (52) holds. A similar procedure should also be performed for the other two cases of along-track and cross track distance bounds to be discussed now.

The necessary condition for calculating the distance bounds of the along-track motion provides the following sixth order polynomial equation to be met

$$\eta_6\,s^6 + \eta_5\,s^5 + \eta_4\,s^4 + \eta_3\,s^3 + \eta_2\,s^2 + \eta_1\,s + \eta_0 = 0 \tag{62}$$

where

$$\eta_0 = -\tau_2 + 2\,\tau_4 - 3\,\tau_6 \tag{63}$$

$$\eta_1 = 2\,\tau_1 + 8\,\tau_3 + 18\,\tau_5 \tag{64}$$

$$\eta_2 = -\tau_2 - 10\,\tau_4 + 45\,\tau_6 \tag{65}$$

$$\eta_3 = 4\,\tau_1 - 60\,\tau_5 \tag{66}$$

$$\eta_4 = \tau_2 - 10\,\tau_4 - 45\,\tau_6 \tag{67}$$

$$\eta_5 = 2\,\tau_1 - 8\,\tau_3 + 18\,\tau_5 \tag{68}$$

$$\eta_6 = \tau_2 + 2\,\tau_4 + 3\,\tau_6 \tag{69}$$

The expressions of τ_0, τ_1, ..., τ_6 are, again, given in the Appendix.

Finally, for the cross-track distance bounds, the necessary condition of Eq. (52) with $\rho_i = \rho_z$ becomes

$$\kappa_4\,s^4 + \kappa_3\,s^3 + \kappa_2\,s^2 + \kappa_1\,s + \kappa_0 = 0 \tag{70}$$

where the constant coefficients $\kappa_0, \kappa_1, \ldots, \kappa_4$ are given by

$$\kappa_0 = -\xi_2 - 2\,\xi_4 \tag{71}$$

$$\kappa_1 = 2\,\xi_1 + 8\,\xi_3 \tag{72}$$

$$\kappa_2 = 12\,\xi_4 \tag{73}$$

$$\kappa_3 = 2\,\xi_1 - 8\,\xi_3 \tag{74}$$

$$\kappa_4 = \xi_2 - 2\,\xi_4 \tag{75}$$

4 Numerical simulations

To verify the effectiveness of the mathematical model exploiting the equinoctial parameters and the proposed methodology for determining the relative distances bounds, two simulation examples are now illustrated, in which both the periodic and quasi-periodic case are considered.

For convenience, introduce a distance unit $\mathrm{DU} \triangleq 1\,\mathrm{au}$, and a time unit $\mathrm{TU} \triangleq \sqrt{(1\,\mathrm{au})^3/\mu_\odot} \simeq 58.132\,\mathrm{days}$ (1 terrestrial year is $2\,\pi\,\mathrm{TU}$), where $\mu_\odot$ is the Sun's gravitational parameter. Assume that the chief is the Earth and the deputy is a spacecraft tracking a circular displaced orbit whose orbital plane is parallel to the $(\hat{\boldsymbol{x}}_I, \hat{\boldsymbol{y}}_I)$ plane with a constant displacement $H_D = 0.02\,\mathrm{au} \simeq 3 \times 10^6\,\mathrm{km}$. Note that in this case $(\hat{\boldsymbol{x}}_{R_C}, \hat{\boldsymbol{y}}_{R_C})$ coincides with the ecliptic plane. This scenario is consistent, for example with an advanced scientific mission whose target is to achieve a broader observable region for the Earth's north pole [24]. The orbital radius of the deputy is set to be $p_D = 0.9998\,\mathrm{au}$ and the initial true longitude of the deputy is assumed slightly different with that of the chief as $L_0 = 100.0297$. The equinoctial elements of the spacecraft and the Earth, calculated at 1 January 2016 using the JPL Planetary and Lunar Ephemerides DE406 model, are summarized in Tab. 1.

4.1 Quasi-periodic case

As far as the quasi-periodic case is concerned, the mean motion of the deputy is assumed to be $n_D = \sqrt{2}\,n_C$. The extreme values of the generic component ρ_i when the radial, along-track and cross-track motions arrive at their boundaries are summarized in Tab. 2, as well as the critical values of the Earth's true

longitude and the deputy's eccentric longitude. Due to the ergodicity of the quasi-periodic relative motion, there exist multiple extreme values, but only the maximum and the minimum values correspond to the real upper and lower bounds. For the radial motion, it is found that $\iota^\star = -0.8127$ and $\upsilon^\star = -0.8127$ from Eqs. (35) and (36), whereas for the along-track motion, $\iota^\star = 0.4047$ and $\upsilon^\star = 2.3596$ from Eqs. (39)-(40).

Figure 3 shows that the three-dimensional relative trajectory is open, but bounded, since the relative motion is quasi-periodic. Fig. 4 shows the corresponding values of the upper and lower bounds of the relative distances as a function of time. Even though it seems that the relative motion arrives at its boundaries at some times, however the actual critical times approach infinity, and the extreme points shown in Fig. 4 are close to (but not coincident with) the boundaries. It has been pointed out in Ref. [25] that for the quasi-periodic motion, each orbit comes arbitrarily close to any given point on the invariant manifold. This does not imply that the relative orbit passes through each point: it just comes arbitrarily close, since the relative motion is ergodic. Therefore, only the critical values of chief's true longitude $L_C^\star$ and the deputy's eccentric longitude $K_D^\star$ are shown in Fig. 4. Clearly, the extreme values (dashed lines) calculated using the semi-analytical model successfully predict the actual relative distances bounds.

Note that the distance ρ_z of the deputy from the ecliptic plane is nearly coincident with the displacement H_D, which coincides with the distance of the deputy's orbital plane from the Sun's barycenter O. In fact, the oscillations in the function $\rho_z = \rho_z(t)$ are due to the fact that the orbital elements of the Earth's orbit in Tab. 1 correspond to a ICRF/J2000.0 reference frame and, for this reason, the ecliptic plane is not exactly coincident with plane $(\hat{\boldsymbol{x}}_I, \hat{\boldsymbol{y}}_I)$,

whereas, by construction (recall that $i_D = 0$), the deputy's orbital plane is parallel to plane $(\hat{\boldsymbol{x}}_I, \hat{\boldsymbol{y}}_I)$.

4.2 1:1 periodic case

In this case we concentrate on the 1:1 periodic relative motion, that is, a situation in which the chief (the Earth) and the deputy (the spacecraft) have the same orbital period ($n_D = n_C$). Using the equinoctial elements given in Tab. 1, it is possible to calculate the critical times when the relative motion arrives at its boundaries and the corresponding extreme values. The results are summarized in Tab. 3.

Figure 5 shows the extreme values (dashed lines) of relative distances (along a time span of 1 year) calculated via the first-order approximate solution (circles), whereas the exact solution (solid lines) is also reported for comparative purposes. The three dimensional periodic relative motion is illustrated in Fig. 6, where the approximate solution is in excellent agreement with the exact one, thus confirming the usefulness of the proposed method.

Figure 6 shows that the relative trajectory of the deputy allows it to permanently stay above the ecliptic plane and, as such, to be able to observe the Earth region around the geographical north pole. In case the mission requires also an observation of the region around the south pole, the deputy's displaced orbit should have an orbital inclination i_D different from zero. For example, assuming $i_D \in [2,\, 12]\,\mathrm{deg}$, the corresponding relative trajectories are summarized in Fig. 7. It can be concluded that, when the inclination is sufficiently different from zero, the deputy is actually able to reach, within one orbit rev-

olution, regions placed both above and below the ecliptic plane. The extreme (maximum and minimum) values of the spacecraft-ecliptic distance ρ_z during the motion are reported in Fig. 8 as a function of i_D. The figure shows a substantially linear variation of ρ_z extremals with the orbital inclination of the deputy. This is due to the near circularity of Earth's orbit and to the (assumed) circularity of deputy's orbit. Note that, when $i_D = 0$, the maximum and minimum distances of the spacecraft from the ecliptic plane are about coincident with the orbital displacement $H_D = 0.02\,\text{au}$, see Tab. 1.

The possibility of varying ρ_z during the motion (when $i_D \neq 0$) allows also the deputy to reach different values of elevation angle θ with respect to the ecliptic plane. In this context θ is the angle between the direction of the relative position vector $\boldsymbol{\rho}$ and the plane $(\hat{\boldsymbol{x}}_{R_C}, \hat{\boldsymbol{y}}_{R_C})$, viz.

$$\tan\theta = \frac{\rho_z}{\sqrt{\rho_x^2 + \rho_y^2}} \tag{76}$$

As is shown in the figure, an elevation angle in the range $\theta \in [-28,\, 34]\,\text{deg}$ (which allows the two Earth's poles to be observed even in the more unfavourable position of the Earth's rotational axis) is obtained with an inclination angle $i_D = 5\,\text{deg}$. Note that the relative motion gradually becomes twisted as i_D increases. However, since only a small orbital eccentricity assumption is required to obtain an approximate analytical solution, the accuracy remains acceptable as it is independent on the other (displaced) orbital elements.

5 Conclusions

The relative motion between two spacecraft tracking heliocentric displaced orbits has been described by means of a set of modified equinoctial elements,

thus providing a parametric representation of the relative distances in the radial, along-track and cross-track directions. The modified equinoctial elements have a geometrical interpretation and serve as a powerful tool for modeling the relative motion between two displaced orbits. At the same time they are useful for removing the singularities in the definition of the line-of-nodes and the argument of perigee in some special cases in which the classic displaced orbital elements fail.

Based on a closed-form solution, the extreme values of relative distance bounds have been calculated analytically for both the quasi-periodic and the periodic case. In particular, for the periodic case, a time-explicit approximate solution has been used to calculate the extreme values of the relative distances.

Some illustrative examples have shown that the semi-analytical methodology is capable of determining the relative distance bounds with little errors. On the other hand, compared with the pure numerical technique, the approach presented in this paper is more efficient in computation, since the lower and upper bounds can be estimated directly with a given set of elements, without the need of integrating the relative equations. A natural extension of this work is to find a concise (approximate) form of the modulus of the relative distance for spacecraft collision avoidance design.

6 Acknowledgements

This work was funded by the National Natural Science Foundation of China (No. 11472213) and Open Research Foundation of Science and Technology in Aerospace Flight Dynamics Laboratory of China (No. 2015afdl016). This work

was also supported by the Chinese Scholarship Council.

7 Appendix: Coefficients in Eqs. (49)–(51)

The relative distances given by Eqs. (49)–(51) depend on coefficients $\sigma_0, \ldots, \sigma_6$, $\tau_0, \ldots, \tau_6$ and $\xi_0, \ldots, \xi_4$, whose expressions are given below

$$\sigma_0 = [(\lambda_1 + \lambda_4)\, \cos\,(l_{C0} - l_{D0}) + (\lambda_2 - \lambda_3)\, \sin\,(l_{C0} - l_{D0})]\,/2 - f_C\,\lambda_5 - g_C\,\lambda_6 - p_C \tag{77}$$

$$\begin{aligned}
\sigma_1 = {} & [\lambda_5 + p_C\,f_C - \lambda_1\,f_D/2 - \lambda_3\,g_D/2 + (\lambda_1 + \lambda_4)\,\sqrt{f_D^2 + g_D^2}\,\cos\,(l_{D0} + M_{D0})\,/4 \\
& + (\lambda_3 - \lambda_2)\,\sqrt{f_D^2 + g_D^2}\,\sin\,(l_{D0} + M_{D0})\,/4]\,\cos\,(l_{C0}) + [\lambda_6 + p_C\,g_C - \lambda_2\,f_D/2 \\
& - \lambda_4\,g_D/2 + (\lambda_2 - \lambda_3)\,\sqrt{f_D^2 + g_D^2}\,\cos\,(l_{D0} + M_{D0})\,/4 \\
& + (\lambda_1 + \lambda_4)\,\sqrt{f_D^2 + g_D^2}\,\sin\,(l_{D0} + M_{D0})\,/4]\,\sin\,(l_{C0}) \\
& + [(\lambda_1 + \lambda_4)\,\sqrt{f_C^2 + g_C^2}\,\cos\,(l_{C0} + M_{C0})\,/2 + (\lambda_2 - \lambda_3)\,\sqrt{f_C^2 + g_C^2}\,\sin\,(l_{C0} + M_{C0})\,/2 \\
& - \lambda_1\,f_C - \lambda_2\,g_C]\,\cos\,(l_{D0}) + [(\lambda_3 - \lambda_2)\,\sqrt{f_C^2 + g_C^2}\,\cos\,(l_{C0} + M_{C0})\,/2 \\
& + (\lambda_1 + \lambda_4)\,\sqrt{f_C^2 + g_C^2}\,\sin\,(l_{C0} + M_{C0})\,/2 - \lambda_3\,f_C - \lambda_4\,g_C]\,\sin\,(l_{D0})
\end{aligned} \tag{78}$$

$$\begin{aligned}
\sigma_2 = {} & [\lambda_6 + p_C\,g_C - \lambda_2\,f_D/2 - \lambda_4\,g_D/2 - (\lambda_1 + \lambda_4)\,\sqrt{f_D^2 + g_D^2}\,\sin\,(l_{D0} + M_{D0})\,/4 \\
& + (\lambda_3 - \lambda_2)\,\sqrt{f_D^2 + g_D^2}\,\cos\,(l_{D0} + M_{D0})\,/4]\,\cos\,(l_{C0}) + [-\lambda_5 - p_C\,f_C + \lambda_1\,f_D/2 \\
& + \lambda_3\,g_D/2 - (\lambda_2 - \lambda_3)\,\sqrt{f_D^2 + g_D^2}\,\sin\,(l_{D0} + M_{D0})\,/4 \\
& + (\lambda_1 + \lambda_4)\,\sqrt{f_D^2 + g_D^2}\,\cos\,(l_{D0} + M_{D0})\,/4]\,\sin\,(l_{C0}) \\
& + [(\lambda_2 - \lambda_3)\,\sqrt{f_C^2 + g_C^2}\,\cos\,(l_{C0} + M_{C0})\,/2 - (\lambda_1 + \lambda_4)\,\sqrt{f_C^2 + g_C^2}\,\sin\,(l_{C0} + M_{C0})\,/2 \\
& - \lambda_3\,f_C - \lambda_4\,g_C]\,\cos\,(l_{D0}) + [(\lambda_1 + \lambda_4)\,\sqrt{f_C^2 + g_C^2}\,\cos\,(l_{C0} + M_{C0})\,/2 \\
& + (\lambda_2 - \lambda_3)\,\sqrt{f_C^2 + g_C^2}\,\sin\,(l_{C0} + M_{C0})\,/2 + \lambda_1\,f_C + \lambda_2\,g_C]\,\sin\,(l_{D0})
\end{aligned} \tag{79}$$

$$\begin{aligned}
\sigma_3 = {} & [(\lambda_1 - \lambda_4)\,\cos\,(l_{C0} + l_{D0}) + (\lambda_2 + \lambda_3)\,\sin\,(l_{C0} + l_{D0})]/2 \\
& + [(\lambda_5 + p_C\,f_C)\,\cos\,(l_{C0} + M_{C0}) + (\lambda_6 + p_C\,g_C)\,\sin\,(l_{C0} + M_{C0})]\,\sqrt{f_C^2 + g_C^2}
\end{aligned} \tag{80}$$

$$\sigma_4 = [(\lambda_2+\lambda_3)\,\cos(l_{C0}+l_{D0}) + (\lambda_4-\lambda_1)\,\sin(l_{C0}+l_{D0})]/2$$
$$+ [(\lambda_6+p_C\,g_C)\,\cos(l_{C0}+M_{C0}) - (\lambda_5+p_C\,f_C)\,\sin(l_{C0}+M_{C0})]\,\sqrt{f_C^2+g_C^2} \tag{81}$$

$$\sigma_5 = [(\lambda_1-\lambda_4)\,\cos(l_{D0}+M_{D0}) + (\lambda_2+\lambda_3)\,\sin(l_{D0}+M_{D0})]\,\sqrt{f_D^2+g_D^2}\,\cos(l_{C0})/4$$
$$+ [(\lambda_2+\lambda_3)\,\cos(l_{D0}+M_{D0}) + (\lambda_4-\lambda_1)\,\sin(l_{D0}+M_{D0})]\,\sqrt{f_D^2+g_D^2}\,\sin(l_{C0})/4$$
$$+ [(\lambda_1-\lambda_4)\,\cos(l_{C0}+M_{C0}) + (\lambda_2+\lambda_3)\,\sin(l_{C0}+M_{C0})]\,\sqrt{f_C^2+g_C^2}\,\cos(l_{D0})/2$$
$$+ [(\lambda_2+\lambda_3)\,\cos(l_{C0}+M_{C0}) + (\lambda_4-\lambda_1)\,\sin(l_{C0}+M_{C0})]\,\sqrt{f_C^2+g_C^2}\,\sin(l_{D0})/2 \tag{82}$$

$$\sigma_6 = [(\lambda_4-\lambda_1)\,\sin(l_{D0}+M_{D0}) + (\lambda_2+\lambda_3)\,\cos(l_{D0}+M_{D0})]\,\sqrt{f_D^2+g_D^2}\,\cos(l_{C0})/4$$
$$+ [-(\lambda_2+\lambda_3)\,\sin(l_{D0}+M_{D0}) + (\lambda_4-\lambda_1)\,\cos(l_{D0}+M_{D0})]\,\sqrt{f_D^2+g_D^2}\,\sin(l_{C0})/4$$
$$+ [(\lambda_4-\lambda_1)\,\sin(l_{C0}+M_{C0}) + (\lambda_2+\lambda_3)\,\cos(l_{C0}+M_{C0})]\,\sqrt{f_C^2+g_C^2}\,\cos(l_{D0})/2$$
$$+ [-(\lambda_2+\lambda_3)\,\sin(l_{C0}+M_{C0}) + (\lambda_4-\lambda_1)\,\cos(l_{C0}+M_{C0})]\,\sqrt{f_C^2+g_C^2}\,\sin(l_{D0})/2 \tag{83}$$

$$\tau_0 = [(\lambda_2-\lambda_3)\,\cos\,(l_{C0}-l_{D0}) - (\lambda_1+\lambda_4)\,\sin\,(l_{C0}-l_{D0})]/2 - f_C\,\lambda_6 + g_C\,\lambda_5 \tag{84}$$

$$\tau_1 = [\lambda_6 - \lambda_2\,f_D/2 - \lambda_4\,g_D/2 + (\lambda_2-\lambda_3)\,\sqrt{f_D^2+g_D^2}\,\cos(l_{D0}+M_{D0})/4$$
$$+ (\lambda_1+\lambda_4)\,\sqrt{f_D^2+g_D^2}\,\sin(l_{D0}+M_{D0})/4]\,\cos(l_{C0}) + [-\lambda_5 + \lambda_1\,f_D/2$$
$$+ \lambda_3\,g_D/2 - (\lambda_1+\lambda_4)\,\sqrt{f_D^2+g_D^2}\,\cos(l_{D0}+M_{D0})/4$$
$$+ (\lambda_2-\lambda_3)\,\sqrt{f_D^2+g_D^2}\,\sin(l_{D0}+M_{D0})/4]\,\sin(l_{C0})$$
$$+ [(\lambda_2-\lambda_3)\,\sqrt{f_C^2+g_C^2}\,\cos(l_{C0}+M_{C0})/2 - (\lambda_1+\lambda_4)\,\sqrt{f_C^2+g_C^2}\,\sin(l_{C0}+M_{C0})/2$$
$$- \lambda_2\,f_C + \lambda_1\,g_C]\,\cos(l_{D0}) + [(\lambda_1+\lambda_4)\,\sqrt{f_C^2+g_C^2}\,\cos(l_{C0}+M_{C0})/2$$
$$+ (\lambda_2-\lambda_3)\,\sqrt{f_C^2+g_C^2}\,\sin(l_{C0}+M_{C0})/2 + \lambda_4\,f_C + \lambda_3\,g_C]\,\sin(l_{D0}) \tag{85}$$

$$\tau_2 = [-\lambda_5 + \lambda_1\, f_D/2 + \lambda_3\, g_D/2 + (\lambda_3 - \lambda_2)\, \sqrt{f_D^2 + g_D^2}\, \sin(l_{D0} + M_{D0})/4$$
$$+ (\lambda_1 + \lambda_4)\, \sqrt{f_D^2 + g_D^2}\, \cos(l_{D0} + M_{D0})/4]\, \cos(l_{C0}) + [-\lambda_6 + \lambda_2\, f_D/2$$
$$+ \lambda_4\, g_D/2 + (\lambda_1 + \lambda_4)\, \sqrt{f_D^2 + g_D^2}\, \sin(l_{D0} + M_{D0})/4$$
$$+ (\lambda_2 - \lambda_3)\, \sqrt{f_D^2 + g_D^2}\, \cos(l_{D0} + M_{D0})/4]\, \sin(l_{C0})$$
$$+ [(\lambda_3 - \lambda_2)\, \sin(l_{C0} + M_{C0}) - (\lambda_1 + \lambda_4)\, \cos(l_{C0} + M_{C0})]\, \sqrt{f_C^2 + g_C^2}\, \cos(l_{D0})/2$$
$$+ [-(\lambda_1 + \lambda_4)\, \sin(l_{C0} + M_{C0}) + (\lambda_2 - \lambda_3)\, \cos(l_{C0} + M_{C0})]\, \sqrt{f_C^2 + g_C^2}\, \sin(l_{D0})/2 \tag{86}$$

$$\tau_3 = [(\lambda_4 - \lambda_1)\, \sin(l_{C0} + l_{D0}) + (\lambda_2 + \lambda_3)\, \cos(l_{C0} + l_{D0})]/2$$
$$- [\lambda_6\, \sin(l_{C0} + M_{C0}) + \lambda_5\, \cos(l_{C0} + M_{C0})]\, \sqrt{f_C^2 + g_C^2} \tag{87}$$

$$\tau_4 = [-(\lambda_2 + \lambda_3)\, \sin(l_{C0} + l_{D0}) + (\lambda_4 - \lambda_1)\, \cos(l_{C0} + l_{D0})]/2$$
$$- [\lambda_6\, \sin(l_{C0} + M_{C0}) + \lambda_5\, \cos(l_{C0} + M_{C0})]\, \sqrt{f_C^2 + g_C^2} \tag{88}$$

$$\tau_5 = [(\lambda_2 + \lambda_3)\, \cos(l_{D0} + M_{D0}) + (\lambda_4 - \lambda_1)\, \sin(l_{D0} + M_{D0})]\, \sqrt{f_D^2 + g_D^2}\, \cos(l_{C0})/4$$
$$+ [(\lambda_4 - \lambda_1)\, \cos(l_{D0} + M_{D0}) - (\lambda_2 + \lambda_3)\, \sin(l_{D0} + M_{D0})]\, \sqrt{f_D^2 + g_D^2}\, \sin(l_{C0})/4$$
$$+ [(\lambda_2 + \lambda_3)\, \cos(l_{C0} + M_{C0}) + (\lambda_4 - \lambda_1)\, \sin(l_{C0} + M_{C0})]\, \sqrt{f_C^2 + g_C^2}\, \cos(l_{D0})/2$$
$$+ [(\lambda_4 - \lambda_1)\, \cos(l_{C0} + M_{C0}) - (\lambda_2 + \lambda_3)\, \sin(l_{C0} + M_{C0})]\, \sqrt{f_C^2 + g_C^2}\, \sin(l_{D0})/2 \tag{89}$$

$$\tau_6 = [-(\lambda_2 + \lambda_3)\, \sin(l_{D0} + M_{D0}) + (\lambda_4 - \lambda_1)\, \cos(l_{D0} + M_{D0})]\, \sqrt{f_D^2 + g_D^2}\, \cos(l_{C0})/4$$
$$+ [(\lambda_1 - \lambda_4)\, \sin(l_{D0} + M_{D0}) - (\lambda_2 + \lambda_3)\, \cos(l_{D0} + M_{D0})]\, \sqrt{f_D^2 + g_D^2}\, \sin(l_{C0})/4$$
$$+ [-(\lambda_2 + \lambda_3)\, \sin(l_{C0} + M_{C0}) + (\lambda_4 - \lambda_1)\, \cos(l_{C0} + M_{C0})]\, \sqrt{f_C^2 + g_C^2}\, \cos(l_{D0})/2$$
$$+ [(\lambda_1 - \lambda_4)\, \sin(l_{C0} + M_{C0}) - (\lambda_2 + \lambda_3)\, \cos(l_{C0} + M_{C0})]\, \sqrt{f_C^2 + g_C^2}\, \sin(l_{D0})/2 \tag{90}$$

$$\xi_0 = \lambda_9 - f_D\,\lambda_7/2 - g_D\,\lambda_8/2 \tag{91}$$

$$\xi_1 = \lambda_7\,\cos\left(l_{D0}\right) + \lambda_8\,\sin\left(l_{D0}\right) \tag{92}$$

$$\xi_2 = \lambda_8\,\cos\left(l_{D0}\right) - \lambda_7\,\sin\left(l_{D0}\right) \tag{93}$$

$$\xi_3 = \left[\lambda_7\,\cos\left(l_{D0}+M_{D0}\right) + \lambda_8\,\sin\left(l_{D0}+M_{D0}\right)\right]\sqrt{f_D^2+g_D^2}/2 \tag{94}$$

$$\xi_4 = \left[\lambda_8\,\cos\left(l_{D0}+M_{D0}\right) - \lambda_7\,\sin\left(l_{D0}+M_{D0}\right)\right]\sqrt{f_D^2+g_D^2}/2 \tag{95}$$

References

[1] R. J. McKay, M. Macdonald, J. Biggs, C. R. McInnes, Survey of highly-non-Keplerian orbits with low-thrust propulsion, Journal of Guidance, Control, and Dynamics 34 (3) (2011) 645–666, doi: 10.2514/1.52133.

[2] J.-Y. Prado, A. Perret, G. Pignolet, Using a solar sail for a plasma storm early warning system, in: W. Burke, T. D. Guyenne (Eds.), Environment Modelling for Space-based Applications, no. ESA SP-392, ESTEC Noordwijk, 1996, pp. 213–223.

[3] M. Ceriotti, J. Heiligers, C. R. McInnes, Trajectory and spacecraft design for a pole-sitter mission, Journal of Spacecraft and Rockets 51 (1) (2014) 311–326, doi: 10.2514/1.A32477.

[4] C. R. McInnes, Near earth object orbit modification using gravitational coupling, Journal of Guidance, Control, and Dynamics 30 (3) (2007) 870–873, doi: 10.2514/1.25864.

[5] S. Gong, J. Li, H. BaoYin, Formation flying solar-sail gravity tractors in displaced orbit for towing near-earth asteroids, Celestial Mechanics and Dynamical Astronomy 105 (2009) 159–177, doi: 10.1007/s10569-009-9211-8.

[6] J. Simo, C. R. McInnes, Feedback stabilization of displaced periodic orbits:

Application to binary asteroids, Acta Astronautica 96 (1) (2014) 106–115, doi: 10.1016/j.actaastro.2013.11.026.

[7] M. MacDonald, R. J. McKay, M. Vasile, F. B. De Frescheville, J. Biggs, C. R. McInnes, Low-thrust-enabled highly-non-keplerian orbits in support of future mars exploration, Journal of Guidance, Control, and Dynamics 34 (5) (2011) 1396–1411, doi: 10.2514/1.52602.

[8] S. K. Borowski, D. R. McCurdy, T. W. Packard, Near earth asteroid human mission possibilities using nuclear thermal rocket (ntr) propulsion, in: 48th AIAA/ASME/SAE/ASEE Joint Propulsion Conference and Exhibit 2012, Atlanta, GA, 2012, paper AIAA-2012-4209.

[9] C. R. McInnes, Passive control of displaced solar sail orbits, Journal of Guidance, Control and Dynamics 21 (6) (1998) 975–982, doi: 10.2514/2.4334.

[10] S. Gong, J. Li, H. Baoyin, Analysis of displaced solar sail orbits with passive control, Journal of Guidance, Control, and Dynamics 31 (3) (2008) 782–785, doi: 10.2514/1.32360.

[11] P. Janhunen, P. K. Toivanen, J. Polkko, S. Merikallio, P. Salminen, E. Haeggstrom, H. Seppanen, R. Kurppa, J. Ukkonen, S. Kiprich, G. Thornell, H. Kratz, L. Richter, O. Kromer, R. Rosta, M. Noorma, J. Envall, S. Latt, G. Mengali, A. A. Quarta, H. Koivisto, O. Tarvainen, T. Kalvas, J. Kauppinen, A. Nuottajarvi, A. Obraztsov, Electric solar wind sail: Towards test missions, Review of Scientific Instruments 81 (11) (2010) 111301 (1–11), doi: 10.1063/1.3514548.

[12] G. Mengali, A. A. Quarta, Non-Keplerian orbits for electric sails, Celestial Mechanics and Dynamical Astronomy 105 (1–3) (2009) 179–195, doi: 10.1007/s10569-009-9200-y.

[13] S. Gong, H. Baoyin, J. Li, Solar sail formation flying around displaced solar

orbits, Journal of Guidance, Control, and Dynamics 30 (4) (2007) 1148–1152, doi: 10.2514/1.24315.

[14] S. Gong, G. Yunfeng, J. Li, Solar sail formation flying on an inclined earth orbit, Acta Astronautica 68 (1-2) (2011) 226–239, doi: 10.1016/j.actaastro.2010.08.022.

[15] W. Wang, J. P. Yuan, G. Mengali, A. A. Quarta, Invariant manifold and bounds of relative motion between heliocentric displaced orbits, Journal of Guidance, Control, and Dynamics 39 (8) (2016) 1764–1776, doi: 10.2514/1.G001751.

[16] W. Wang, G. Mengali, A. A. Quarta, J. P. Yuan, Extreme values of relative distances for spacecraft in elliptic displaced orbits, Advances in Space Research 58 (4) (2016) 475–487, doi: 10.1016/j.asr.2016.05.007.

[17] T. Fukushima, New two-body regularization, The Astronomical Journal 133 (1) (2007) 1–10, doi: 10.1086/509606.

[18] G. R. Hintz, Survey of orbit element sets, Journal of Guidance, Control, and Dynamics 31 (3) (2008) 785–790, doi: 10.2514/1.32237.

[19] M. J. H. Walker, J. Owens, B. Ireland, A set of modified equinoctial orbit elements, Celestial Mechanics 36 (4) (1985) 409–419, doi: 10.1007/BF01227493.

[20] M. J. H. Walker, A set of modified equinoctial orbit elements (erratum), Celestial Mechanics 38 (4) (1986) 391–392, doi: 10.1007/BF01238929.

[21] S. Greenstreet, B. Ngo, H. asnd Gladman, The orbital distribution of near-earth objects inside earth's orbit, Icarus 217 (1) (2012) 355–366, doi: 10.1016/j.icarus.2011.11.010.

[22] P. A. Abell, B. W. Barbee, P. W. Chodas, J. Kawaguchi, R. R. Landis, D. D. Mazanek, P. Michel, Asteroids IV, 2nd Edition, The University of Arizona Press, 2016, Ch. 5, pp. 855–881, ISBN: 978-0816532131.

[23] R. H. Battin, An Introduction to the Mathematics and Methods of Astrodynamics, AIAA, New York, 1987, pp. 210, 490–494, ISBN: 1-563-47342-9.

[24] M. Ceriotti, J. Heiligers, C. R. McInnes, Novel pole-sitter mission concepts for continuous polar remote sensing, in: Sensors, Systems, and Next-Generation Satellites XVI, Vol. 8533, Edinburgh, United Kingdom, 2012.

[25] S. H. Strogatz, Nonlinear Dynamics and Chaos, Perseus Books, Reading, Massachusetts, 1994, pp. 273–276.

List of Tables

	p [au]	H [au]	f	g	h	k	L_0 [deg]
chief	0.9995	0	-3.3706×10^{-3}	1.6133×10^{-2}	-1.5156×10^{-5}	-1.4669×10^{-5}	99.7640
deputy	0.9998	0.02	0	0	0	0	100.0297

Table 1
Equinoctial elements of the chief (Earth at January 1, 2016 in ICRF/J2000.0) and the deputy spacecraft.

component	$\iota^\star$	$\upsilon^\star$	$L_C^\star \bmod \pi$ [rad]	$K_D^\star \bmod \pi$ [rad]	extreme values [au]	
ρ_x	-0.8127	-0.8127	1.7767	1.7767	0.0165	-2.0160
ρ_y	0.4047	2.3596	0.7691	2.3399	0.9998	-0.9998
ρ_z	–	–	–	2.3399	0.02004	0.01996

Table 2
Extreme values of relative distances for the quasi-periodic case with $n_D/n_C = \sqrt{2}$.

component	$s^\star$		$t^\star \bmod 2\,\pi$ [TU]		extreme values [au]	
ρ_x	-7.152	0.1398	0.2778	3.4194	0.0069	-0.0274
ρ_y	-1	1	4.7124	1.5708	0.1752	0.11
ρ_z	-4.6914	0.2132	0.42	3.5616	0.02004	0.01996

Table 3
Extreme values of relative distances for the 1:1 periodic case.

List of Figures

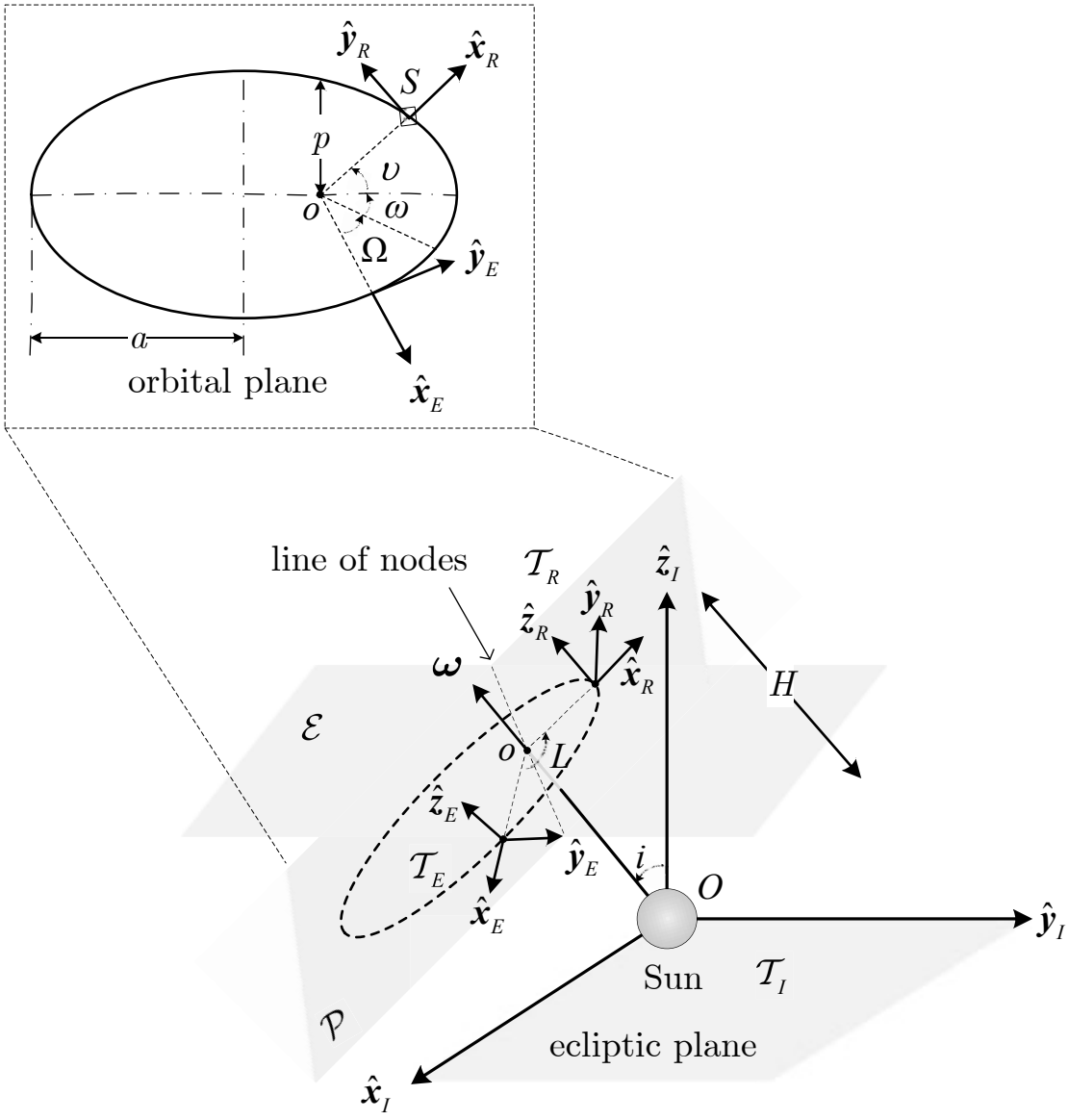

Figure 1. Reference frames and characteristic angles (adapted from Ref. [16]).

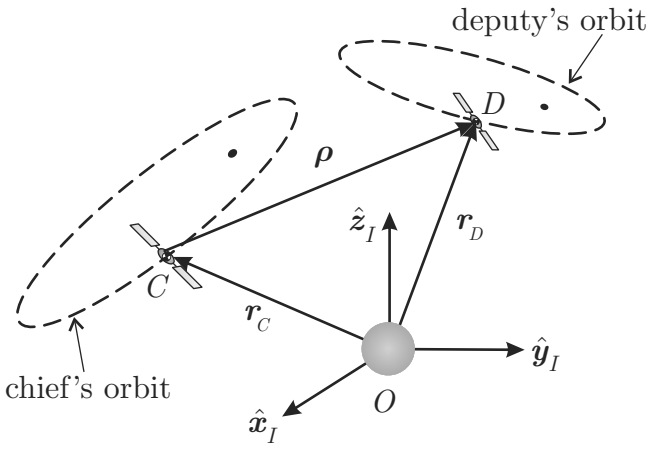

Figure 2. Displaced orbits of chief and deputy spacecraft.

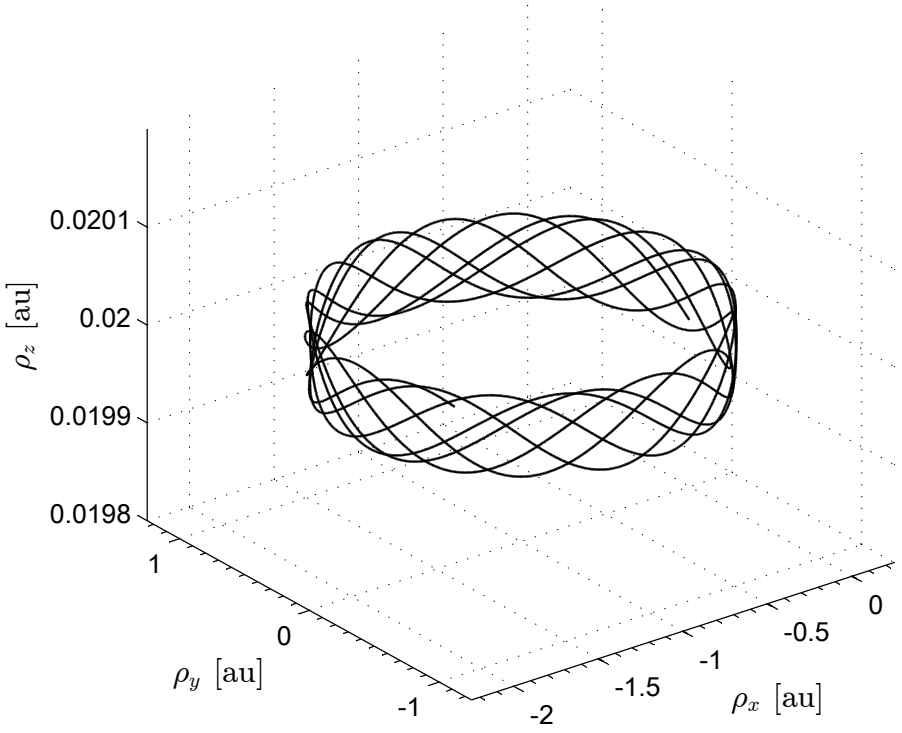

Figure 3. Relative trajectory in a quasi-periodic case with $n_D/n_C = \sqrt{2}$.

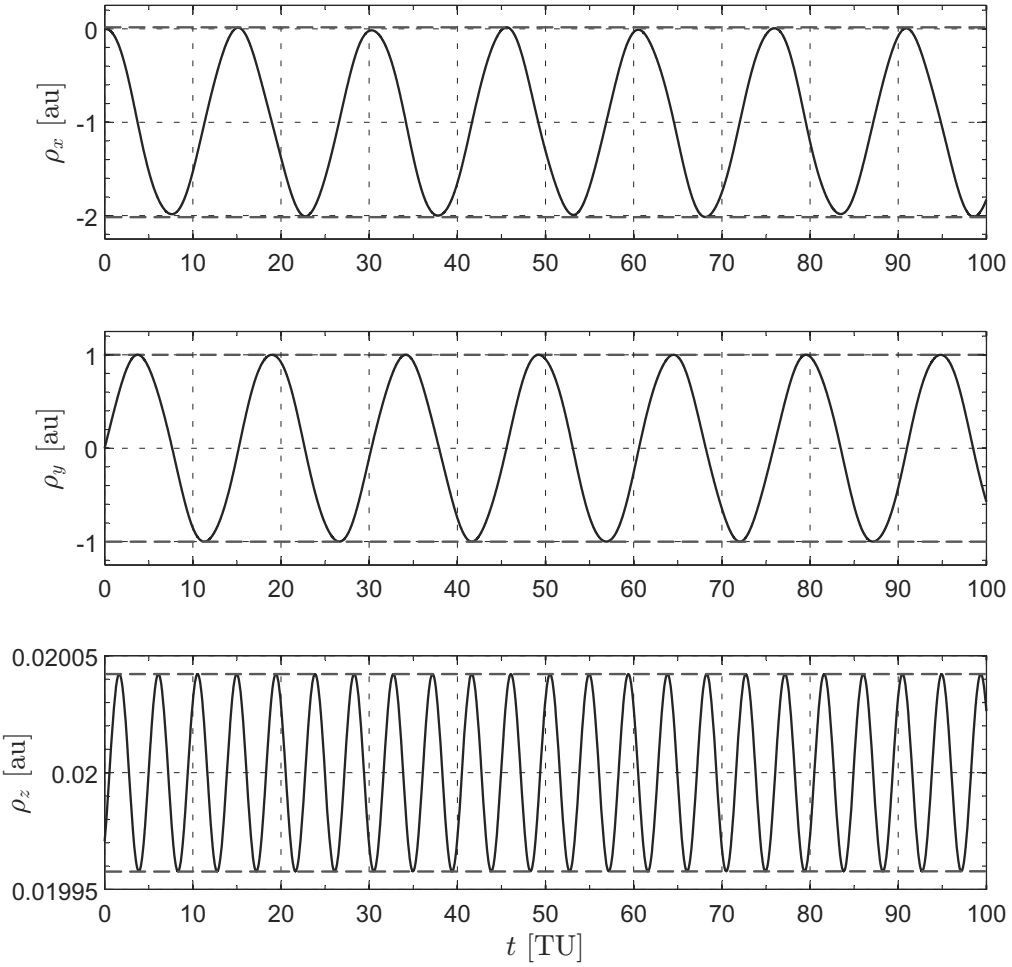

Figure 4. Components of the relative position vector in a quasi-periodic case with $n_D/n_C = \sqrt{2}$.

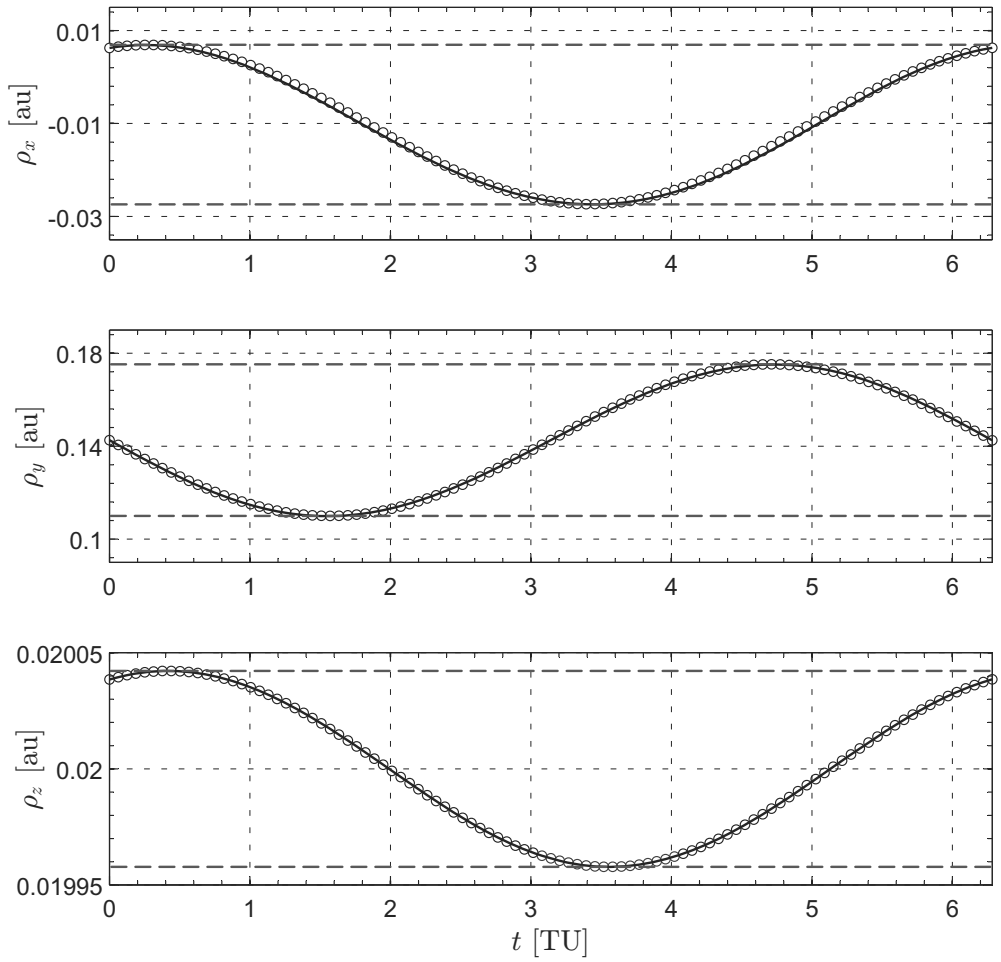

Figure 5. Components of the relative position vector in a 1:1 periodic case over a time span of 1 year: approximate (circles) vs. exact (solid line) solution.

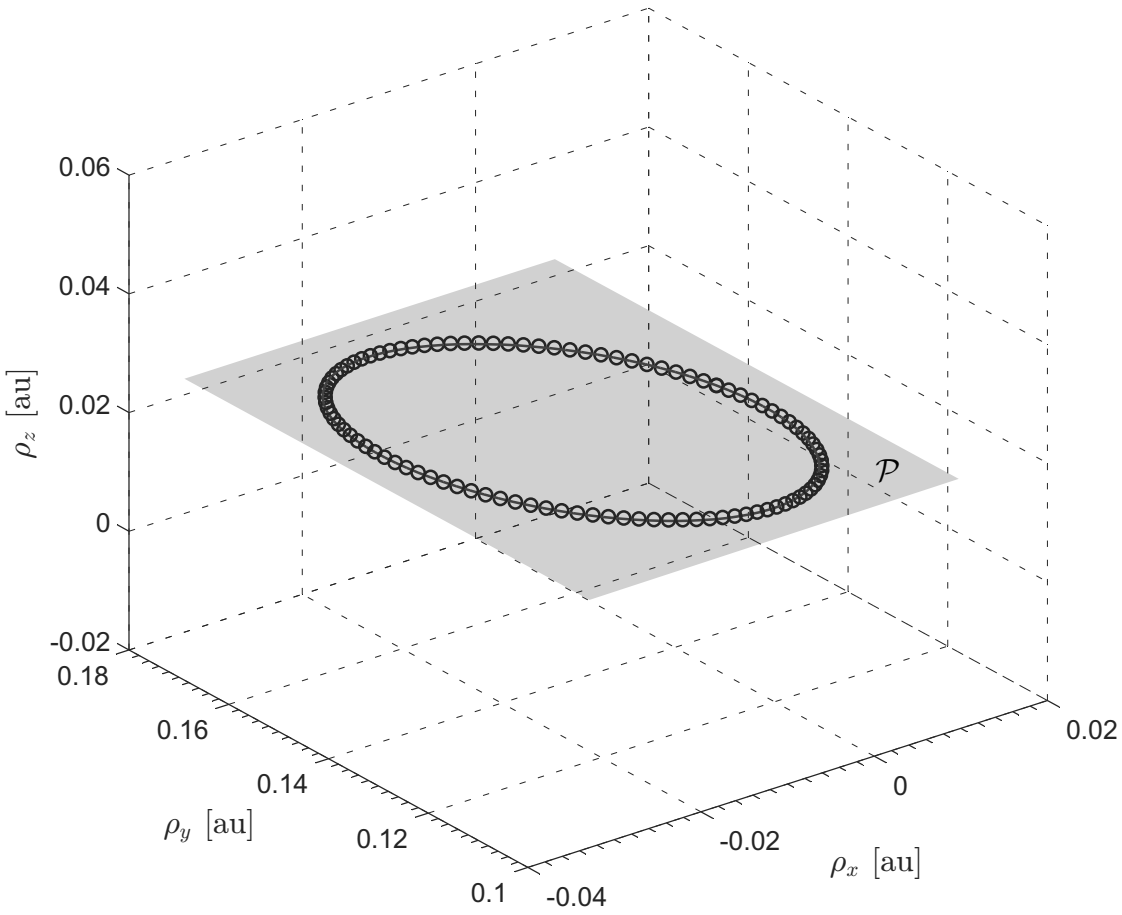

Figure 6. Relative trajectory in 1:1 periodic case: approximate (circles) vs. exact (solid line) solution.

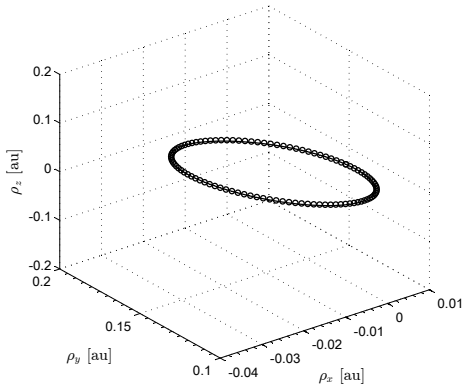

(a) $i_D = 2\,\text{deg}$.

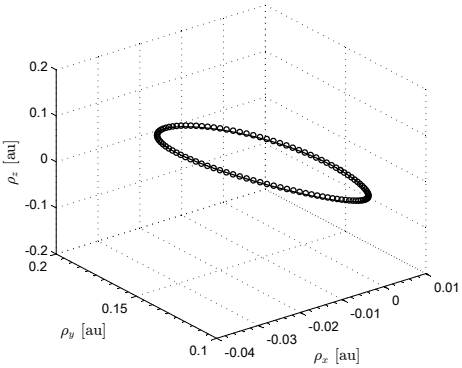

(b) $i_D = 4\,\text{deg}$.

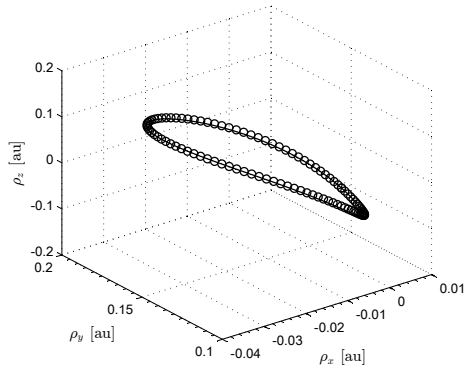

(c) $i_D = 6\,\text{deg}$.

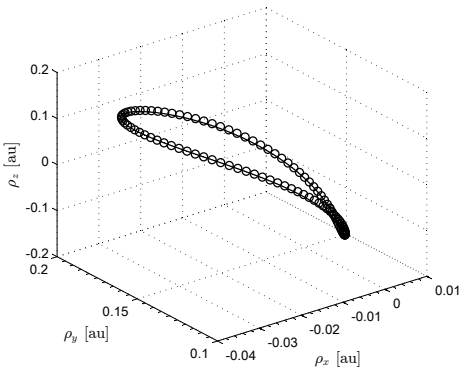

(d) $i_D = 8\,\text{deg}$.

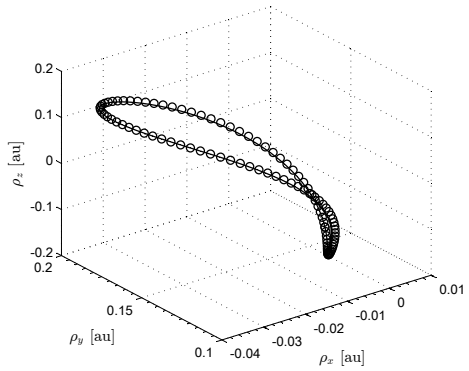

(e) $i_D = 10\,\text{deg}$.

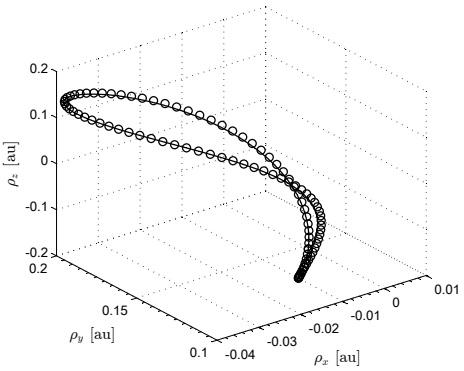

(f) $i_D = 12\,\text{deg}$.

Figure 7. Relative trajectory in 1:1 periodic case as a function of the deputy's orbital inclination: approximate (circles) vs. exact (solid line) solution.

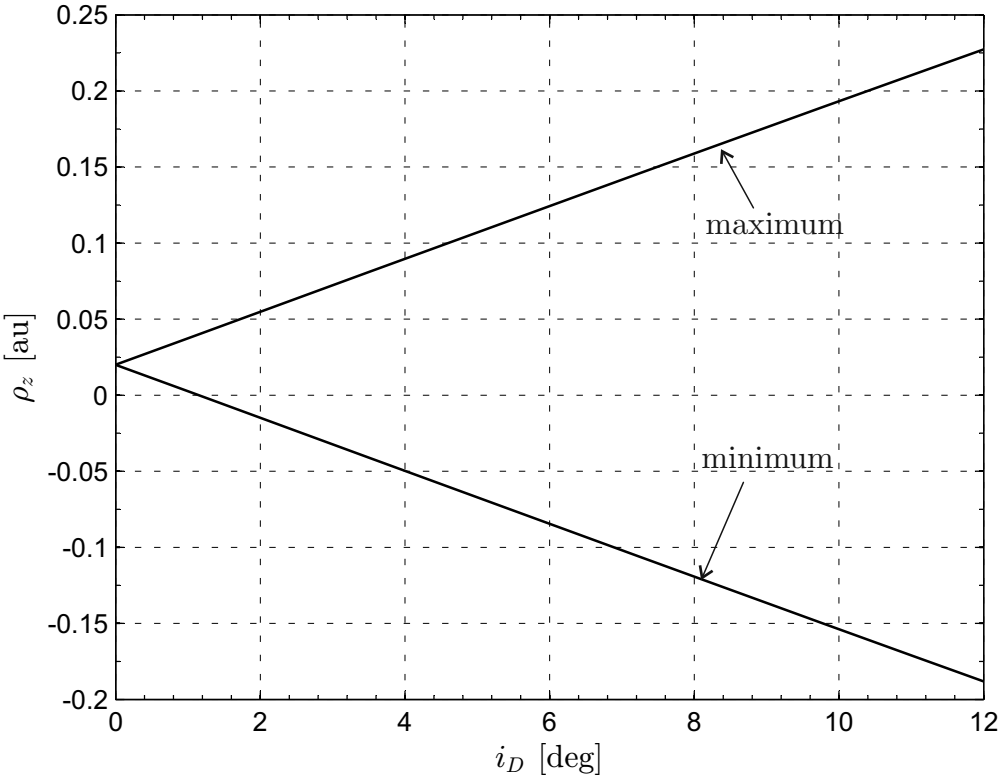

Figure 8. Extreme values of the deputy-ecliptic distance ρ_z as a function of the orbital inclination i_D.

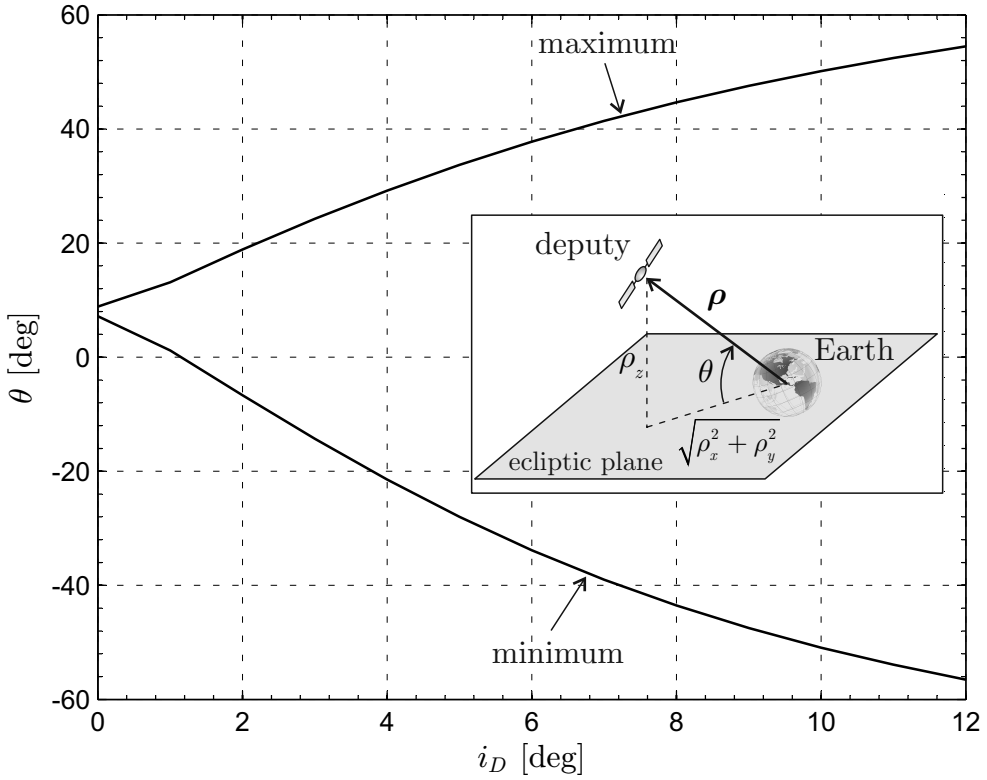

Figure 9. Extreme values of the deputy's elevation angle θ as a function of the orbital inclination i_D.